

On the Generation and Maintenance of the 2012/13 Sudden Stratospheric Warming

FEN XU

Institute of Space Weather, School of Mathematics and Statistics, Nanjing University of Information Science and Technology, and Nanjing Movelaser Technology Co., Ltd., Nanjing, China

X. SAN LIANG

School of Marine Sciences, and School of Atmospheric Sciences, Nanjing University of Information Science and Technology, Nanjing, China

(Manuscript received 4 January 2017, in final form 4 July 2017)

ABSTRACT

Using a newly developed analysis tool, multiscale window transform (MWT), and the MWT-based localized multiscale energetics analysis, the 2012/13 sudden stratospheric warming (SSW) is diagnosed for an understanding of the underlying dynamics. The fields are first reconstructed onto three scale windows: that is, mean window, sudden warming window or SSW window, and synoptic window. According to the reconstructions, the major warming period may be divided into three stages: namely, the stages of rapid warming, maintenance, and decay, each with different mechanisms. It is found that the explosive growth of temperature in the rapid warming stage (28 December–10 January) results from the collaboration of a strong poleward heat flux and canonical transfers through baroclinic instabilities in the polar region, which extract available potential energy (APE) from the mean-scale reservoir. In the course, a portion of the acquired APE is converted to and stored in the SSW-scale kinetic energy (KE), leading to a reversal of the polar night jet. In the stage of maintenance (11–25 January), the mechanism is completely different: First the previously converted energy stored in the SSW-scale KE is converted back, and, most importantly, in this time a strong barotropic instability happens over Alaska–Canada, which extracts the mean-scale KE to maintain the high temperature, while the mean-scale KE is mostly from the lower atmosphere, in conformity with the classical paradigm of mean flow–wave interaction with the upward-propagating planetary waves. This study provides an example that a warming may be generated in different stages through distinctly different mechanisms.

1. Introduction

The sudden stratospheric warming (SSW), or simply sudden warming, refers to the phenomenon of an abrupt temperature rise by several tens of kelvins in a short period in the high latitudes of the stratosphere, and, in most extreme cases, a reversal of zonal-mean westerly winds associated with the stratospheric polar night jet [see [Butler et al. \(2015\)](#) and references therein]. Discovered in 1952 by the German scientist Richard Scherhag when analyzing radiosonde data; it has been linked to other atmospheric phenomena such as the quasi-biennial oscillation (QBO) ([Gray et al. 2004](#); [Charyulu et al. 2007](#)), North Atlantic Oscillation (NAO) [particularly the negative NAO phase ([Baldwin and Dunkerton 2001](#))], and ENSO teleconnection ([Ineson and Scaife 2009](#); [Butler et al. 2014](#)), and has been

evidenced to impact the Atlantic storm track ([Thompson et al. 2002](#)), equatorial tropospheric convective activity ([Kodera 2006](#)), Arctic and Antarctic ozone variability ([Schoeberl and Hartmann 1991](#)), transport of tropospheric CO₂ and pollutants ([Jiang et al. 2013](#)), North Atlantic Ocean circulation ([Reichler et al. 2012](#)), and tropospheric planetary and synoptic-scale eddies ([Hitchcock and Simpson 2016](#)), to name a few. It may exert an effect on our daily lives by warming Greenland, eastern Canada, and southern Eurasia and bringing about extreme cold air outbreaks in parts of North America and Eurasia (e.g., [Thompson et al. 2002](#); [Nath et al. 2016](#)).

An attempt to give the SSW an unambiguous definition turns out to be challenging. For over 60 years, scientists have been endeavoring to define and characterize it but still have not reached an agreement. In their comprehensive review, [Butler et al. \(2015\)](#) remarked that a well-accepted definition, and hence classification,

Corresponding author: X. San Liang, sanliang@courant.nyu.edu

is “at best ambiguous and at worst nonexistent.” Usually referred to in the literature are major warming and minor warming, plus additional ones, such as Canadian warming. [Note, here we should distinguish SSW and stratospheric final warming (SFW); the latter is characteristic of the breakdown of the polar vortices (Black et al. 2006; Black and McDaniel 2007; Sheshadri et al. 2014)]. In such characterizing, a significant rise in temperature is generally required, but in recent decades zonal wind reversal has been the dominant basis for the definition of major warmings (e.g., McInturff 1978). These discrepancies have led to different SSW identifications. For example, application of the seven different definitions described in Butler et al. (2015) to the 1958–2014 NCEP Reanalysis data results in 26–46 major SSWs, or 0.46–0.8 per winter. In this study, it is not our intention to run into the debate of the definition; we will focus on one major warming event, namely, the December 2012–January 2013 SSW, which has been unanimously identified by all the seven definitions in Butler et al. (2015). We want particularly to investigate how the temperature is abruptly increased.

Since the discovery of the SSW event, much effort has been invested in explaining its generating mechanism. Classically it is believed that SSWs are due to the interaction of the upward-propagating planetary waves (Charney and Drazin 1961; Dickinson 1968) with the zonal winds. Specifically, the waves from the troposphere act to decelerate the polar night jet, giving rise to the distortion/breakdown of the polar vortex (Matsuno 1970, 1971). This wave–mean flow interaction is illustrated in the semispectral model of Holton (1976, 1980); it has been further studied by Robinson (1985, 1988) and evidenced in other studies, such as that of Harada et al. (2010).

On the other hand, Trenberth (1973) found that the nonzonal heating may also account for a weaker westerly jet and a considerable warming in the polar night stratosphere, while Sjöberg and Birner (2012) emphasized the role of transient forcing and, particularly, the scale of transient forcing. They found that the frequency of SSW occurrences drops as the temporal forcing scale is reduced.

Apart from the external formation mechanisms, in another line of work it is suggested that SSWs may have intrinsic origins; they can occur without precursor tropospheric pulse of planetary wave energy. The self-tuned resonance mechanism (Plumb 1981; McIntyre 1982; Dritschel and McIntyre 2008; Esler and Matthewman 2011; Matthewman and Esler 2011; Albers and Birner 2014) and catastrophe theory (Chao 1985) are such examples. Plumb (1981) pointed out that the temporal growth could result from the

resonance between the stationary waves and the slowing-down progressive waves and that the SSWs with the polar vortex displaced and those with the polar vortex split must have quite different generating mechanisms. To understand how nature may select the mechanism(s) for the SSW formation, dynamical diagnostics make an important methodology. Particularly, the Lorenz energy cycle diagnostics prove to be a powerful approach (Lorenz 1955). In this regard, the energetics were first studied by Reed et al. (1963), and this was followed by Julian and Labitzke (1965), Perry (1967), and Trenberth (1973), among others. These multiscale energetics studies, however, are all global in that the resulting energetics are averaged over the domain of concern, without distinguishing between spatial locations. The limitation of global energetics has long been recognized, and there has been a long-lasting effort to overcome this by introducing local energetics studies, such as those of Holopainen (1978), Plumb (1983), and, recently, Liang and Robinson (2005), Murakami (2011), and Liang (2016). [Particularly, the empirical method of Murakami (2011) was applied by Zuo et al. (2012) to study the January 2009 sudden warming event.]

The difficulty of energetics analysis lies in the following two aspects. First, atmospheric processes tend to occur locally in time; an SSW event spans a short period in the year and is not stationary even during that period. The time-mean decomposition essentially cannot have nonstationary processes appropriately separated. An alternative is to take zonal mean, but that invokes another issue: that is, a loss of spatial localization in longitude. Besides, atmospheric processes usually involve more than just two ranges of scales. Now a common practice is to rely on filters to achieve the decomposition. However, how filtered fields can be used to express multiscale energy and energetic terms (any quadratic properties) is by no means trivial; actually, it is a profound problem in functional analysis. This is because filtered fields are reconstructions in physical space, while multiscale energy is a concept in phase space that is related to physical energy through the renowned Parseval relation (cf. Liang and Anderson 2007). The second difficulty is the relaxation of the global integration/average from the Lorenz-type energetic terms. It has long been argued that the thus-obtained energetics, particularly the energy transfers between the mean and eddy fields that are most important in the energy cycle diagnostics, are ambiguous (Holopainen 1978, Plumb 1983). Furthermore, the widely used transfer (i.e., the energy extraction via Reynolds stress against basic profile) does not yield the expected diagnosis with benchmark problems

(Liang and Robinson 2007); see the following section for more details.

Recently it has been found that the above two difficulties actually can be overcome in a unified approach [see Liang (2016) for a review] within the framework of a newly developed functional analysis apparatus called multiscale window transform (MWT; Liang and Anderson 2007). Liang and Anderson realized that, for some specially devised orthogonal filters, a filtered field has correspondingly a transform coefficient, just like that in Fourier transform and inverse Fourier transform. It has been proved that the transform coefficient then can be combined to represent the multiscale energetics. Using this, Liang (2016) rigorously proved, through a reconstruction of some atomlike quantities, that the transfer processes can be unambiguously separated from the intertwined nonlinear transports. The resulting transfers bear a Lie bracket form, just like the Poisson bracket in Hamiltonian mechanics. This formalism, which was first proposed in Liang and Robinson (2005) in a half-empirical way (rigorously proved later on), has led to a new diagnostic methodology, namely, the localized multiscale energy and vorticity analysis (MS-EVA). MS-EVA has been applied with success in many real oceanic and atmospheric diagnoses and engineering problems, such as wake control (e.g., Liang and Wang 2004). See section 2 for a brief introduction.

We will apply the new multiscale energetics formalism to diagnose the SSW processes. We choose a particular case (i.e., the December 2012–January 2013 SSW case) for this purpose. This SSW has been identified by all the seven definitions listed in Butler et al. (2015); it is very special in that, in the course of warming, the polar vortex is not only displaced but also split. Since 1980, there are only three cases (1985/86, 1987/88, and 2012/13) that are like this one (Liu and Zhang 2014; Nath et al. 2016). Besides, this event has an extraordinarily long duration. According to Nath et al. (2016), it lasts for more than 38 days, greatly exceeding the climatological mean. For this reason, there have been many studies with this case (e.g., Liu and Zhang 2014; Tripathi et al. 2016; Coy et al. 2015; De Wit et al. 2015; Taguchi 2016; Nath et al. 2016; Attard et al. 2016). A faithful energetics diagnosis is expected to help us gain more understanding of this unusual event.

In the following, we first briefly introduce the MWT-based multiscale energetics analysis (i.e., MS-EVA), and then the data that will be used (section 3). The MS-EVA is set up in section 4, and sections 5 and 6 provide the analysis results. This study is summarized in section 7.

2. A brief introduction of multiscale window transform and localized multiscale energetics

As we know, a formalism of multiscale energetics from time averaging does not have information in time, while that from zonal averaging loses information in longitude. During the past decades, it has been a common practice to use filters to reformulate the problem. However, how energy should be represented with the filtered fields has become a fundamental problem. For example, if a field $u(t)$ is decomposed with a filter into a basic part \bar{u} and an eddy part u' , where both \bar{u} and u' are functions of t , then what is the eddy energy? It is by no means as trivial as $(u')^2$, as has been widely used in the literature. To illustrate, suppose we have a simple Fourier expansion

$$\begin{aligned} u(t) &= \bar{u}(t) + u'(t) \\ &= (a_0 \cos t + b_0 \sin t) + (a_1 \cos 100t + b_1 \sin 100t), \end{aligned}$$

where the subscripts 0 and 1 represent the slow- and fast-scale processes, respectively. Now what are the energies for these processes? During the past 2–3 decades, it has become a common practice that they are simply taken as

$$\begin{aligned} [\bar{u}(t)]^2 &= [a_0 \cos t + b_0 \sin t]^2 \quad \text{and} \\ [u'(t)]^2 &= (a_1 \cos 100t + b_1 \sin 100t)^2. \end{aligned}$$

This is, unfortunately, conceptually wrong. We know, for this simple example, the energies should be, respectively,

$$a_0^2 + b_0^2 \quad \text{and} \quad a_1^2 + b_1^2.$$

That is to say multiscale energy is a concept with the Fourier coefficients in phase space, which is related to its physical space counterpart through the Parseval equality in mathematical analysis. It is the square of the norm of a field, and physically it can be interpreted as the Fourier transform of an autocorrelation function (e.g., Batchelor 1953). When \bar{u} is a constant, it can be easily proved that $a_1^2 + b_1^2 = [u'(t)]^2$, just as that with the Reynolds decomposition. This also explains why the time averaging in the classical energetic formalism cannot be removed, although it causes the resulting energetics to lose information in time.

As we see, it is a rather profound problem to have the local energy of a time-dependent filtered field faithfully represented. In fact, this issue has just been addressed in the development of MWT (Liang and Anderson 2007), with the aid of the established connection between filter banks and wavelets (Strang and Nguyen 1997).

MWT is a functional analysis tool that decomposes a function space into a direct sum of orthogonal subspaces, each with an exclusive range of scales (in time or in space, depending on the problem in question), while preserving its local properties. Such a subspace is termed a *scale window*, or simply a window. MWT is developed for a faithful representation of the multiscale energies on the resulting scale windows and hence make multiscale energetics analysis possible. This is a feature lacked in the traditional filters, the outputs of which are fields in physical space, while multiscale energy is a concept in phase space that is related to its physical space counterpart through the Parseval equality. Liang and Anderson (2007) realized that, just as in the Fourier transform and inverse Fourier transform, there exists a transfer-reconstruction pair for a class of specially devised orthogonal filters. This pair is the very MWT and its peer [i.e., multiscale window reconstruction (MWR)]. Loosely speaking, the MWR of a series $S(t)$ results in a filtered series, while the corresponding MWT coefficients can give the energy of that filtered series. For a brief introduction, see the section 2 of Liang (2016).

In MWT, a scale window is bounded below and above by two scale levels. For a series with a time duration of τ , a scale level j corresponds to a period $2^{-j}\tau$. The time steps of the series hence need to total to a number of the power of 2. In this study, as discussed in section 4, we impose three scale windows that characterize, respectively, the background fields, the fields on the scales of SSW events, and the field on smaller scales. They are between scale levels $0-j_0$, j_0-j_1 , and j_1-j_2 . For the sake of easy reference, we will denote them with $\varpi = 0, 1$, and 2 and refer to them as the mean or background window, SSW window or window of sudden warming, and synoptic window, respectively. Later on in the next section these scale levels will be determined based on the time scales of SSWs and synoptic processes.

Given a time series $[S(t)]$, application of MWT yields the MWT coefficient, which we will write as \hat{S}_n^{ϖ} where $(\hat{\cdot})_n^{\varpi}$ denotes MWT on window ϖ at time step n , and through MWR we obtain a reconstruction on window ϖ , written $S^{\varpi}(t)$. Here the tilde in the superscript is originally used in constructing the MWT (Liang and Anderson 2007) and has been a convention ever since. It is used to indicate that the MWT is for a range of scales, rather than for a specific scale, as in other transforms (such as wavelet transform). Besides, it is used so to avoid confusion with notations that do not carry meaning of transform and/or reconstruction [e.g., the kinetic energy on scale window ϖ in Eq. (6) below]. By a theorem called the property of marginalization, Liang and Anderson (2007) proved that the energy on window ϖ is proportional to $\hat{S}_n^{\varpi 2}$. {Note it is by no means as trivial as

$[S^{\varpi}(t)]^2$.} For a dry atmosphere, the multiscale kinetic energy (KE) and available potential energy (APE) are then proportional to $\hat{\mathbf{v}}_h^{\varpi} \cdot \hat{\mathbf{v}}_h^{\varpi}$ and $(\hat{T}^{\varpi})^2$, respectively, where \mathbf{v} is velocity, T is temperature, and the subscript h indicates horizontal component; more details are included in Table 1.

Now consider the primitive equations in an isobaric coordinate frame:

$$\frac{\partial \mathbf{v}_h}{\partial t} + \mathbf{v}_h \cdot \nabla_h \mathbf{v}_h + \omega \frac{\partial \mathbf{v}_h}{\partial p} + f \mathbf{k} \times \mathbf{v}_h = -\nabla_h \Phi + \mathbf{F}_{m,p} + \mathbf{F}_{m,h}, \quad (1)$$

$$\frac{\partial \Phi}{\partial p} = -\alpha, \quad (2)$$

$$\nabla_h \cdot \mathbf{v}_h + \frac{\partial \omega}{\partial p} = 0, \quad (3)$$

$$\frac{\partial T}{\partial t} + \mathbf{v}_h \cdot \nabla_h T + \omega \frac{\partial T}{\partial p} + \omega \bar{\alpha} \frac{L - L_d}{g} + \omega \alpha \frac{L - L_d}{g} = \frac{\dot{q}_{\text{net}}}{c_p}, \quad (4)$$

and

$$\alpha = \frac{R}{P} T, \quad (5)$$

where L is the lapse rate and L_d the lapse rate for dry air, and overbar stands for horizontal and time mean. The other notations are conventional. Note here the geopotential and specific volume are anomaly fields: that is, the time mean over the period of concern has been removed. From these equations, the multiscale KE and APE are found to be governed by

$$\frac{\partial K^{\varpi}}{\partial t} + \nabla \cdot \mathbf{Q}_K^{\varpi} = \Gamma_K^{\varpi} - \nabla \cdot \mathbf{Q}_P^{\varpi} - b^{\varpi} + F_{K,P}^{\varpi} + F_{K,h}^{\varpi}, \quad (6)$$

$$\frac{\partial A^{\varpi}}{\partial t} + \nabla \cdot \mathbf{Q}_A^{\varpi} = \Gamma_A^{\varpi} + b^{\varpi} + S_A^{\varpi} + F_A^{\varpi}, \quad (7)$$

for windows $\varpi = 0, 1$, and 2 , where the expressions for the symbols are listed in Table 1. Note here the time step n has been suppressed for notational simplicity. For convenience, the divergence terms $\nabla \cdot \mathbf{Q}_A^{\varpi}$, $\nabla \cdot \mathbf{Q}_K^{\varpi}$, and $\nabla \cdot \mathbf{Q}_P^{\varpi}$ will be hereinafter written as ΔQ_A^{ϖ} , ΔQ_K^{ϖ} , and ΔQ_P^{ϖ} , respectively. Among these terms, the transfer Γ is very different from those in classical formalisms. Particularly, it has an interesting property: that is,

$$\sum_{\varpi} (\sum_n \Gamma_n^{\varpi}) = 0 \quad (8)$$

(now n is supplied), as first shown in Liang and Robinson (2005) and later on rigorously proved (see Liang 2016). Physically, this means that the energy transfer is a mere redistribution of energy among the scale windows, without generating or destroying energy as a whole. This

TABLE 1. Multiscale energetic terms ($m^2 s^{-3}$) in Eqs. (6) and (7). If total energetics (W) are to be computed, the resulting integrals with respect to ($x, y,$ and p) should be divided by g . Besides, all terms are to be multiplied by $2^{1/2}$, which is omitted for notational simplicity.

K^ϖ	$\frac{1}{2} \widehat{\mathbf{v}}_h^{\sim\varpi} \cdot \widehat{\mathbf{v}}_h^{\sim\varpi}$	KE on scale window ϖ
\mathbf{Q}_K^ϖ	$\frac{1}{2} (\widehat{\mathbf{v}\mathbf{v}}_h)^{\sim\varpi} \cdot \widehat{\mathbf{v}}_h^{\sim\varpi}$	Flux of KE on window ϖ
Γ_K^ϖ	$\frac{1}{2} [(\widehat{\mathbf{v}\mathbf{v}}_h)^{\sim\varpi} : \nabla \widehat{\mathbf{v}}_h^{\sim\varpi} - \nabla \cdot (\widehat{\mathbf{v}\mathbf{v}}_h)^{\sim\varpi} \cdot \widehat{\mathbf{v}}_h^{\sim\varpi}]$	Canonical transfer of KE to window ϖ
\mathbf{Q}_P^ϖ	$\widehat{\mathbf{v}}^{\sim\varpi} \widehat{\Phi}^{\sim\varpi}$	Pressure flux
b^ϖ	$\widehat{\omega}^{\sim\varpi} \widehat{\alpha}^{\sim\varpi}$	Buoyancy conversion
A^ϖ	$\frac{1}{2} c (\widehat{T}^{\sim\varpi})^2, c = \frac{g}{\overline{T}(g/c_p - L)}$	APE on scale window ϖ
\mathbf{Q}_A^ϖ	$\frac{1}{2} c \widehat{T}^{\sim\varpi} (\widehat{\mathbf{v}T})^{\sim\varpi}$	Flux of APE on window ϖ
Γ_A^ϖ	$\frac{c}{2} [(\widehat{\mathbf{v}T})^{\sim\varpi} \cdot \nabla \widehat{T}^{\sim\varpi} - \widehat{T}^{\sim\varpi} \nabla \cdot (\widehat{\mathbf{v}T})^{\sim\varpi}]$	Canonical transfer of APE to window ϖ
S_A^ϖ	$\frac{1}{2} \widehat{T}^{\sim\varpi} (\widehat{\omega T})^{\sim\varpi} \frac{\partial c}{\partial p} + \frac{1}{\overline{T}} (\widehat{\omega\alpha})^{\sim\varpi}$	Apparent source–sink (usually negligible)

property, though simply stated, does not hold in previous energetics formalisms (see below). To distinguish it, Γ is termed ‘‘canonical transfer.’’ Besides, it has an expression in a Lie bracket form that satisfies the Jacobian identity, reminiscent of the Poisson bracket in Hamiltonian mechanics [see Liang (2016) for details].

To demonstrate how a canonical transfer differs from the energy transfer in classical energetic formalisms, consider the problem within the traditional Reynolds-decomposition framework. Consider a passive tracer T (may be any scalar field; need not be temperature) in an incompressible flow and neglect diffusion for simplicity:

$$\frac{\partial T}{\partial t} + \nabla \cdot (\mathbf{v}T) = 0, \tag{9}$$

whose decomposed equations are

$$\frac{\partial \overline{T}}{\partial t} + \nabla \cdot (\overline{\mathbf{v}T} + \overline{\mathbf{v}'T'}) = 0 \quad \text{and} \tag{10}$$

$$\frac{\partial T'}{\partial t} + \nabla \cdot (\overline{\mathbf{v}'T'} + \overline{\mathbf{v}T'} + \mathbf{v}'T' - \overline{\mathbf{v}'T'}) = 0. \tag{11}$$

Multiplying Eq. (10) by \overline{T} , and Eq. (11) by T' , and taking the mean, one arrives at the evolutions of the mean energy and eddy energy (variance) (e.g., Pope 2003):

$$\frac{\partial \overline{T^2}/2}{\partial t} + \nabla \cdot (\overline{\mathbf{v}T^2}/2) = -\overline{T\nabla \cdot (\overline{\mathbf{v}'T'})} \quad \text{and} \tag{12}$$

$$\frac{\partial \overline{T'^2}/2}{\partial t} + \nabla \cdot (\overline{\mathbf{v}'T'^2}/2) = -\overline{\mathbf{v}'T'} \cdot \nabla \overline{T}. \tag{13}$$

The terms in divergence form are generally understood as the transports of the mean and eddy energies and those on the right-hand side as the respective energy transfers. The latter are usually used to explain the dynamical source of the mean–eddy interaction. Particularly, when T is a

velocity component, the right side of Eq. (13), $R = -\overline{\mathbf{v}'T'} \cdot \nabla \overline{T}$, has been interpreted as the rate of energy extracted by Reynolds stress, or Reynolds stress extraction for short, against the mean field to fuel the eddy growth; in the context of turbulence research, it is also referred to as the ‘‘rate of the turbulence production’’ (Pope 2003). It has also been extensively utilized in dynamic meteorology to explain phenomena such as cyclogenesis and eddy shedding. However, Holopainen (1978) and Plumb (1983) found that the transport–transfer separation is not unique, and hence the resulting transfer seems to be ambiguous. Moreover, Eqs. (12) and (13) do not, in general, sum to zero on the right-hand side. This is not what one would expect of an energy transfer, which by physical intuition should be a redistribution of energy among scale/scale windows and should not generate nor destroy energy as a whole.

With the MS-EVA formalism, these issues disappear. In this special case, the energy equations are, in contrast to Eqs. (12) and (13),

$$\frac{\partial \overline{T^2}/2}{\partial t} + \nabla \cdot \left(\frac{1}{2} \overline{\mathbf{v}T^2} + \frac{1}{2} \overline{T \mathbf{v}'T'} \right) = -\Gamma \quad \text{and} \tag{14}$$

$$\frac{\partial \overline{T'^2}/2}{\partial t} + \nabla \cdot \left(\frac{1}{2} \overline{\mathbf{v}'T'^2} + \frac{1}{2} \overline{T \mathbf{v}'T'} \right) = \Gamma, \tag{15}$$

where $\Gamma = (1/2)[\overline{T\nabla \cdot (\overline{\mathbf{v}'T'})} - (\overline{\mathbf{v}'T'}) \cdot \nabla \overline{T}]$. Now one can see that the right-hand side is balanced. We hence call this Γ a canonical transfer. As shown by Liang (2016), it has a Lie bracket form. Previously, Liang and Robinson (2007) illustrated, for a benchmark hydrodynamic instability model whose instability structure is analytically known, the traditional Reynolds stress extraction does not give the correct source of instability, while Γ does.

The MS-EVA Eqs. (6) and (7) are thus fundamentally different from the classical ones. By collecting the

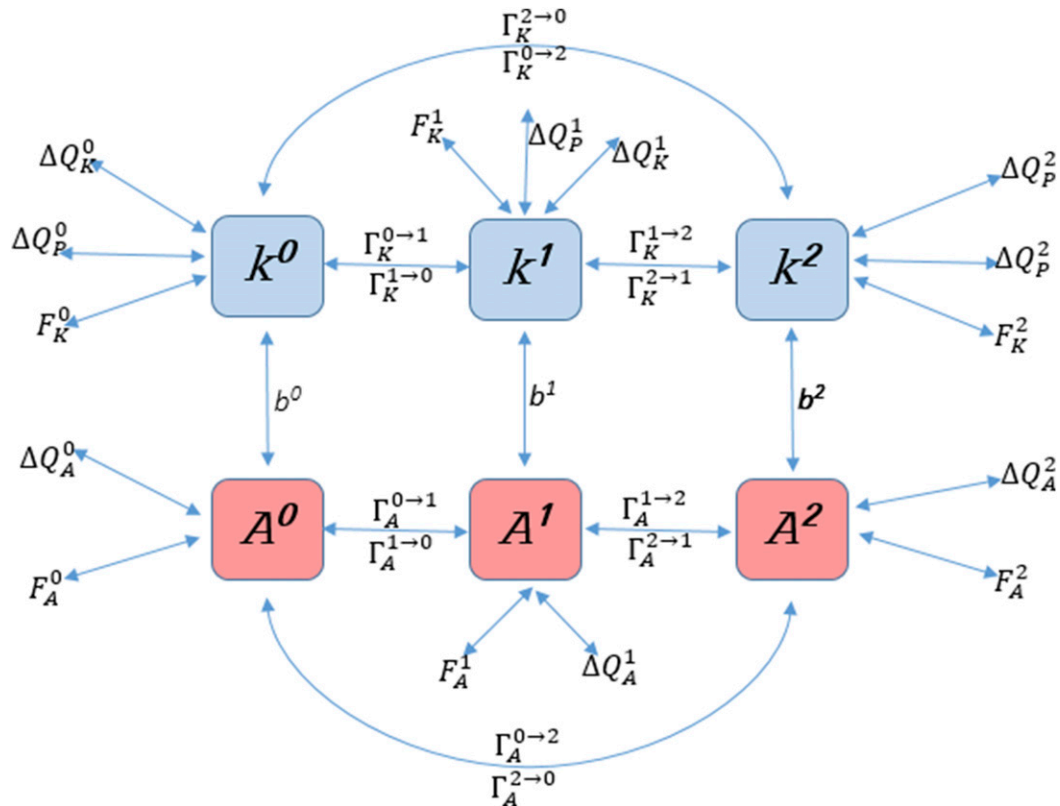


FIG. 1. Energy flowchart for a three-window decomposition. The superscripts 0, 1, and 2 stand for the mean, SSW, and synoptic-scale windows, respectively. The values ΔQ_K^σ , ΔQ_A^σ , and ΔQ_P^σ signify $\nabla \cdot \mathbf{Q}_K^\sigma$, $\nabla \cdot \mathbf{Q}_A^\sigma$, and $\nabla \cdot \mathbf{Q}_P^\sigma$, and the other symbols are explained in Table 1.

MS-EVA terms, the energetic processes can be classified into four categories: energy transport (flux divergence), canonical transfer, buoyancy conversion, and dissipation/diffusion. Interestingly, the first three are all in some conservative form: a transport vanishes if integrated over a closed domain, a canonical transfer vanishes if summarized over windows and locations, while a buoyancy conversion mediates between KE and APE within each individual window. Figure 1 schematizes these processes with a three-window decomposition.

Note a canonical transfer to a window ϖ may involve contributions from different sources. Take the SSW window ($\varpi = 1$) for example: the energy can be from window 0, 2, and even itself, $\varpi = 1$. Notice that, from Table 1, both Γ_K^1 and Γ_A^1 can be expressed as a linear combination of terms in the following triple product form:

$$\Gamma_n^1 = \hat{\mathcal{R}}_n^{-1}(\widehat{pq})_n^{-1}.$$

It then suffices to consider Γ_n^1 only. As established in Liang (2016), it can be decomposed as

$$\Gamma_n^1 = \hat{\mathcal{R}}_n^{-1} \left[(\widehat{p^{\sim 0}q^{\sim 0}})_n^{-1} + (\widehat{p^{\sim 0}q^{\sim 1}})_n^{-1} + (\widehat{p^{\sim 1}q^{\sim 0}})_n^{-1} \right] + \hat{\mathcal{R}}_n^{-1} \left[(\widehat{p^{\sim 1}q^{\sim 2}})_n^{-1} + (\widehat{p^{\sim 2}q^{\sim 1}})_n^{-1} + (\widehat{p^{\sim 2}q^{\sim 2}})_n^{-1} \right] + \hat{\mathcal{R}}_n^{-1} \left[(\widehat{p^{\sim 0}q^{\sim 2}})_n^{-1} + (\widehat{p^{\sim 2}q^{\sim 0}})_n^{-1} \right] + \hat{\mathcal{R}}_n^{-1} \left[(\widehat{p^{\sim 1}q^{\sim 1}})_n^{-1} \right],$$

where the first term on the right-hand side, $\hat{\mathcal{R}}_n^{-1}[(\widehat{p^{\sim 0}q^{\sim 0}})_n^{-1} + (\widehat{p^{\sim 0}q^{\sim 1}})_n^{-1} + (\widehat{p^{\sim 1}q^{\sim 0}})_n^{-1}] = \Gamma^{0 \rightarrow 1}$, is the canonical energy transfer from window 0 to window 1. The second term, denoted by $\Gamma^{2 \rightarrow 1}$, is the energy transfer from window 2 to window 1. The other two are usually very small. More details

are available in Liang (2016). Liang and Robinson (2007) established that $\Gamma^{0 \rightarrow 1}$ is related to the instability of the mean flow, and, in particular, $\Gamma_A^{0 \rightarrow 1}$ and $\Gamma_K^{0 \rightarrow 1}$ are related to, respectively, the baroclinic and barotropic instabilities in geophysical fluid dynamics.

3. Data

The data we will be using are the reanalysis product ERA-Interim provided by the European Centre for Medium-Range Weather Forecasts (ECMWF), including temperature, geopotential, and wind (u , v , ω). The time resolution is 6 h. Vertically there are 37 levels, from 1000 to 1 hPa. In the horizontal direction, we will use a resolution of $2^\circ \times 2^\circ$ for the sake of computational economy. We have also tried the $1^\circ \times 1^\circ$ resolution, and the results are similar.

4. MS-EVA setup

To set up the MS-EVA, we first need to determine the scale window bounds. This is achieved through wavelet spectral analysis. Choose a series of temperature at the North Pole spanning April 2010–November 2015 with a time step of 6 h. We remove the mean over the duration and consider only the temperature anomaly. This totals to $2^{13} = 8192$ data points. (MWT requires that the number of time steps be a power of 2.) This series has the period of concern (January 2013) lying in the middle, with two ends far away enough to avoid the possible boundary effect.

The wavelet power spectrum [with respect to the orthonormal basis built by Liang and Anderson (2007)] is shown in Fig. 2. Also shown is the time series. From the spectrum, clearly there are two peaks. One is at $j = 2$, corresponding to a period of 365.2 days, which is the very annual signal. Another corresponds to the SSW event, $j = 5-8$ (11.4–91.3 days). We have also tried Fourier spectral analysis, but only the annual signal stands out; the SSW signal is mostly disguised. This is a very good example against using Fourier analysis for nonstationary signals.

Based on the above results, we identify three bounds $j_0 = 4$, $j_1 = 8$, and $j_2 = j_{\max} = 13$. They divide the spectrum into three scale windows, which we will refer to as, respectively, mean window, sudden-warming-scale window (or SSW window), and synoptic-scale window. From this, the SSW window contains signals with periods from 16 to 256 days. The mean-scale, SSW-scale, and synoptic-scale reconstructions of the series are shown in Figs. 3a–c. Clearly we can see the annual cycle in Fig. 3a and the sudden warming events in Fig. 3b. Figure 3c shows the temperature variabilities associated with the synoptic eddies.

5. The 2013 SSW fields and their reconstructions

a. A brief description of the original fields

In Fig. 3, we show the temperature evolutions at the North Pole. Figure 3d is the zoom of the period 1 December 2012–9 February 2013. Clearly, in early January

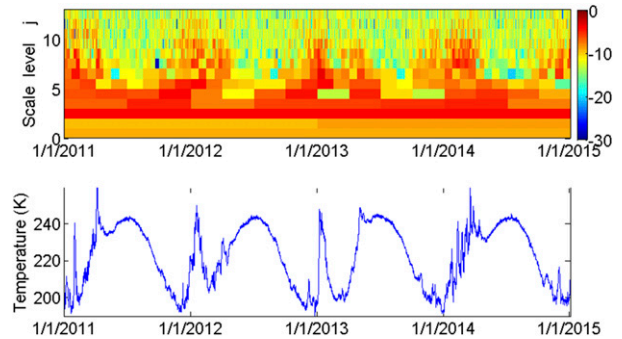


FIG. 2. (top) Wavelet spectrum for the (bottom) 10-hPa polar temperature time series. The mean has been removed prior to the spectral analysis.

2013, the expected low temperature is replaced by a high temperature (the blue solid line in the figure). The warming is so rapid that the temperature anomaly is increased from -25 K on 1 January to 25 K (comparable to the highest of the year) on 6 January. During 7–12 January, it oscillates within a small range. After that, it begins to decline. Besides this major warming, from the figure we see there exist actually two minor warmings early in December and around 24 December. The zonal winds change correspondingly. We look at the 10-hPa wind at 84°N , 180° . In Fig. 3d, a positive value indicates a westerly wind. One can see that, during the period of the sudden warming, the zonal wind is weakened greatly. By 7 January, the westerly wind at 84°N , 180° has essentially changed to an easterly wind.

The evolution of the spatial distribution is shown in Fig. 4. Early in December 2012, the polar region at 10 hPa is occupied by a large-scale cold center, which lies more in the Atlantic Ocean sector. A warm center first appears over the Eurasian continent. As time goes by, it moves poleward; in the meantime, the cold center moves toward the Western Hemisphere. As of 29 December, the warm center reaches 60°N . It develops rapidly in the following days, covering Siberia and the region to the north. The cold center appears in the form of a comma, pushed by the developing warming center to North America, making a dipolar structure in the polar region. As the warm center is pushed northward, the cold center in the Western Hemisphere is split into two halves. By 9 January, the temperature field in the polar region is characterized by two pairs of cold–warm dipoles. The cold centers lie over Alaska and Atlantic–western Europe, while the warm centers are over the European continent and Canada. Afterward, the Eurasian warm center gets weakened and moves toward Canada, which is eventually merged with the warm center on 21 January. Clearly, this process is very special in that the polar

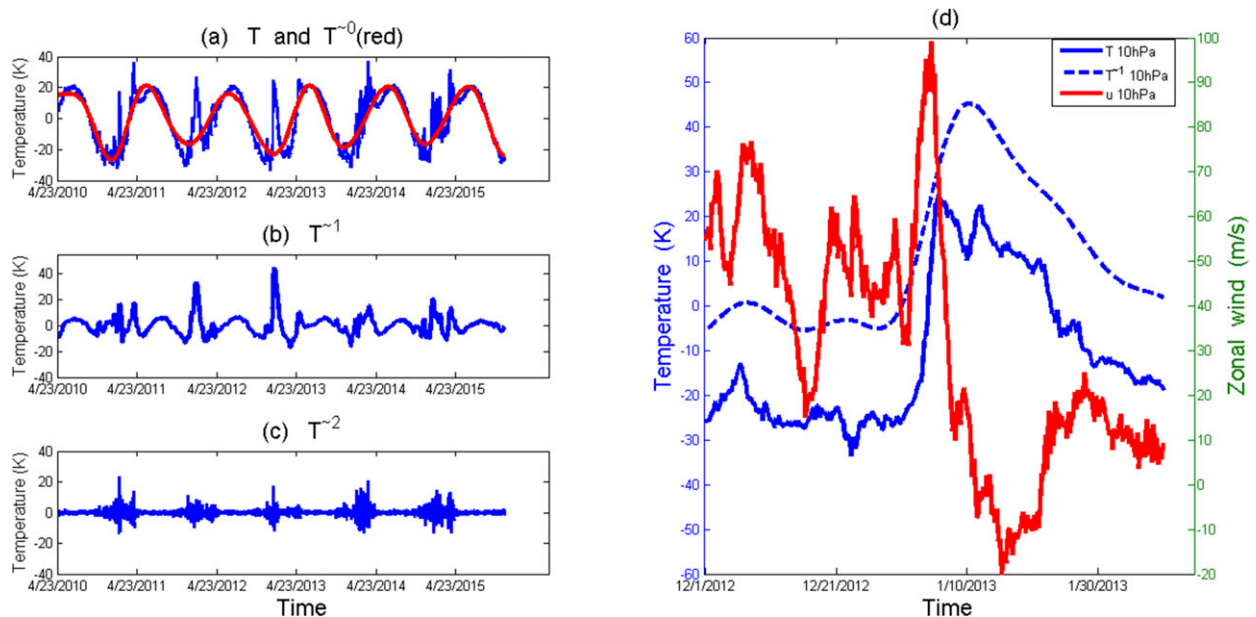


FIG. 3. (a) The temperature anomaly T (in blue; with the mean over 23 Apr 2010–30 Nov 2015 removed) at the North Pole and 10 hPa from 23 Apr 2010 to 30 Nov 2015, and its mean-scale reconstruction (in red), (b) SSW-scale reconstruction, and (c) synoptic-scale reconstruction. The scale window bounds are referred to in the text. (d) The zoom of the above in the period 1 Dec 2012–9 Feb 2013 with the blue solid line being the T in (a), the blue dashed line the T in (b), and the red line the u wind component at 10 hPa.

vortex is not just displaced but also split into two and then four vortices.

b. Multiscale reconstructions

The multiscale reconstructions of the temperature, wind, and geopotential fields on the three scale windows, especially on the sudden warming window, allow us to visualize better the warming event. To get a feeling of this, Fig. 5 shows a snapshot of the decomposition of the 10-hPa temperature in the Northern Hemisphere on 4 January 2013. Obviously, the mean or background field T^{-0} (Fig. 5b) is characterized by a single cold center, and the SSW part T^{-1} is characterized by a single warm center (Fig. 5c). Note on the T^{-0} field the polar vortex is not centered at the pole; in boreal winter, it sits more over the Atlantic side because of the Aleutian high (e.g., O'Neill et al. 2015).

The decomposed temperature fields at 10 hPa evolve differently in different windows. In the mean-scale window there is only a slowly varying cold polar vortex, which lies over Greenland. This feature is just like that in Fig. 5b and hence is not shown here. The varying background implies that the warming process is nonstationary.

In the sudden-warming-scale window, as shown in Fig. 6, a warm center first appears on 21 December, which moves poleward as time goes by, and then extends throughout the whole polar region. This process culminates on 12–14 January, after which the warm center

moves to the Western Hemisphere. Prior to the arrival of the warming early in December, on the SSW scale there appears an obvious cold center over the Eurasian continent (Fig. 6a). If we examine the temperature reconstruction in this scale window for a year without SSW, generally there are no such strong centers. This shows that, during a warming period, some places may actually experience a cooling. This cooling phenomenon has also been identified prior to many other warming events over the past 35 years from the 10-hPa temperature time series at locations (say, 60°N , 180°). A careful discussion, however, is left to future studies.

The evolution of the 10-hPa SSW-scale zonal wind is shown in Fig. 7. In late December on the SSW window, the midstratosphere is still controlled by a westerly wind anomaly. But an easterly wind anomaly, though weak, begins to develop over South Asia and Canada. The easterly wind anomaly is strengthened rapidly in early January and soon takes over the region north of 60°N . It completely replaces the polar westerly wind anomaly on 7 January.

Shown in Fig. 8 is the 10-hPa geopotential field on the SSW-scale window. Its evolution is consistent with the SSW-scale temperature. Prior to the sudden warming, there is a negative center over the polar region. On 14 December, a positive center first appears over Canada. This steers the polar vortex toward Siberia. Afterward, the polar vortex grows and migrates toward Greenland (8–18 January) and then becomes gradually

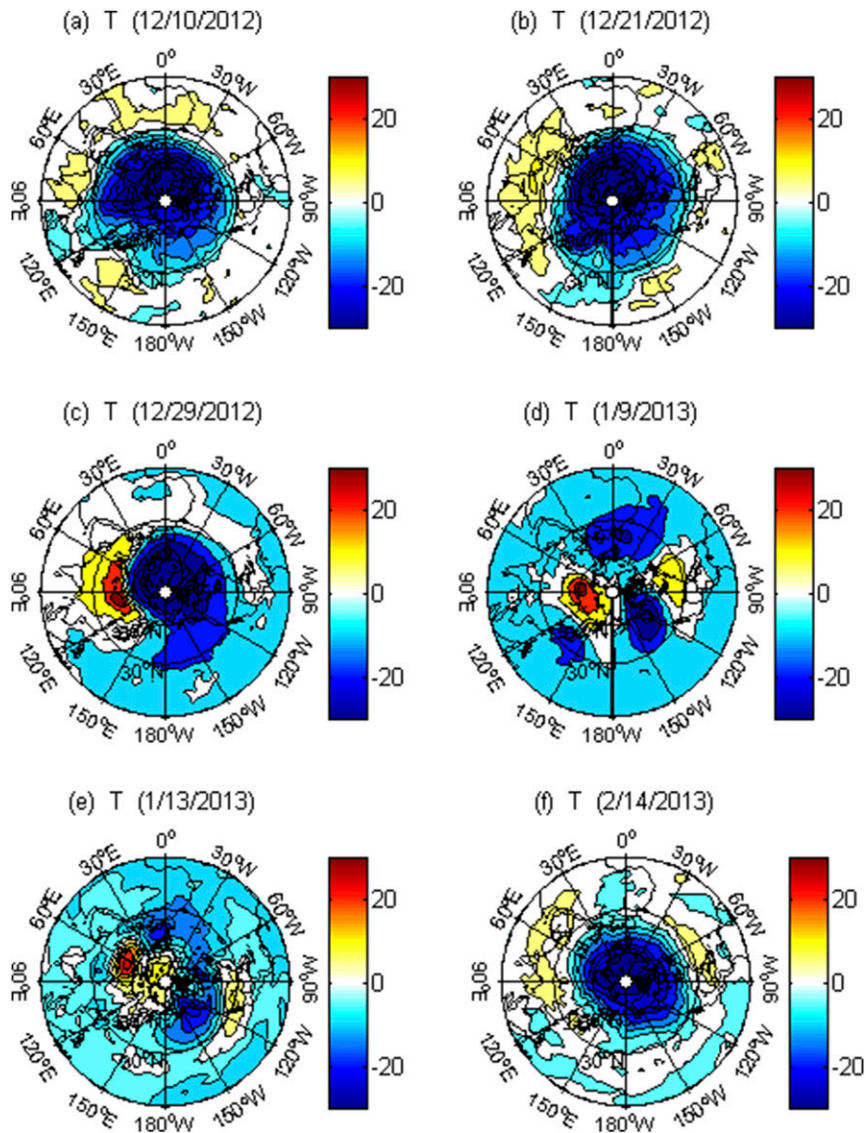


FIG. 4. Temperature anomaly (K) at 10 hPa in the Northern Hemisphere; (a),(b),(c): 10, 21, and 29 Dec 2012; (d),(e): 9 and 13 Jan 2013; and (f) 14 Feb 2013.

weakened. The whole process comes to an end in late February and then completely disappears on the SSW window (until the next warming event).

6. Energetics

a. Sudden-warming-scale energy

Generally, on the SSW-scale window, KE and APE have distributions similar to zonal wind and temperature, respectively (not shown). To show their vertical distribution evolutions, we integrate them on the pressure levels over the whole Northern Hemisphere and plot the results in Fig. 9 (the integration is over the

spherical surface with the meridional weight taken into account). As shown in Fig. 9a, the SSW-scale APE is limited in December–January above 100 hPa, and mostly above 30 hPa. In contrast, besides the maxima in the vertical, the SSW-scale KE has, at 50–5 hPa, three peaks in its evolution: one in early December, one in late December, and the strongest in January.

b. Multiscale energy cycles

1) SSW-SCALE ENERGETIC BALANCE

To better understand the processes underlying the warming event, we integrate the energetic terms over the Northern Hemisphere from 60° to 84°N, and from

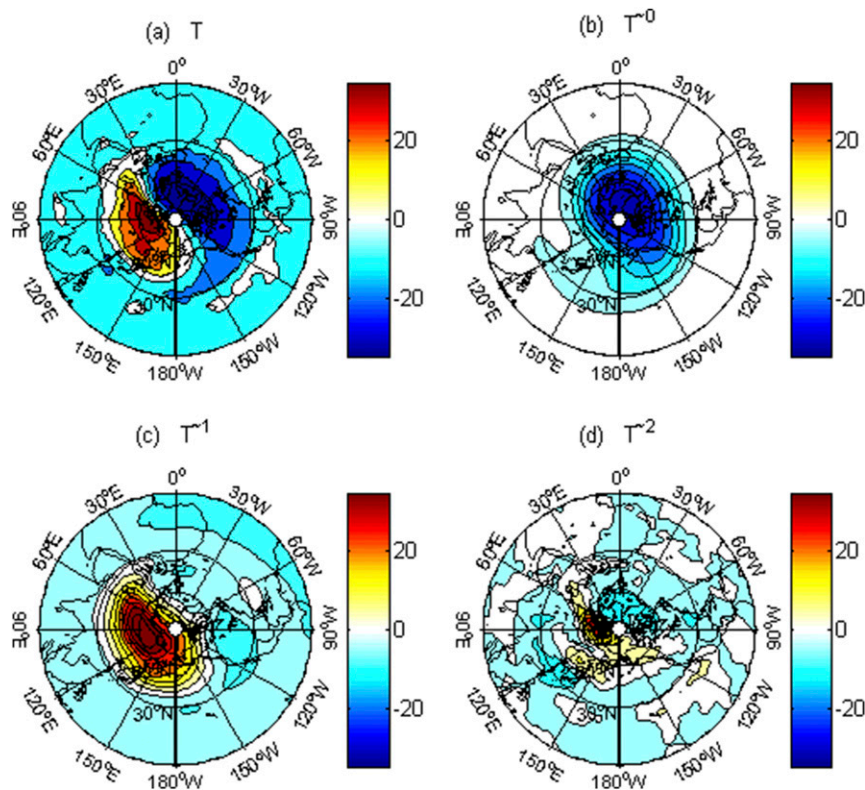


FIG. 5. (a) The 10-hPa temperature anomaly (K) on 4 Jan 2013, and (b) its reconstructions in the mean window, (c) SSW-scale window, and (d) synoptic-scale window.

100 to 10 hPa. (We do not choose 90°N since the pole is a singular point.) The vertical integration is with respect to pressure, and hence the final result should be divided by g to ensure that the energetics have the units of energy change rate [see Liang (2016) for details]. We have also tried the integration from 30° to 84°N ; the resulting bulk energetics are similar.

Notice that the sudden warming is essentially about the APE burst on the SSW window; we hence pay special attention to the SSW window energetics. Figure 10 displays the time evolution of the bulk SSW-scale energetic terms during the period 1 December 2012–9 February 2013. For comparison, superimposed is a time series of the SSW-scale temperature at the pole averaged over 60° – 84°N , 100–10 hPa (blue dashed line). From Fig. 10 (top panel), the APE balance on the SSW window is mainly among buoyancy conversion, transport, and baroclinic canonical transfer. For the SSW-scale KE (middle panel), the balance is among pressure work, buoyancy conversion, and barotropic canonical transfer. The residuals account for the dissipation and other unresolved processes and are generally small. Note that throughout the duration the time rates of change of APE and KE are well correlated (bottom panel of Fig. 10). Besides, the former is in phase with b^1 , indicating the importance of buoyancy

conversion. From the figure, the averaged SSW-scale polar temperature generally follows the variation of ΔQ_P^1 , the pressure working rate, but is out of phase with ΔQ_A^1 , the transport of APE on the SSW window.

2) ENERGY FLOW PATHS IN DIFFERENT STAGES

We use the above polar temperature time series to divide the duration 1 December 2012–9 February 2013 into four subperiods: 1–27 December, 28 December–10 January, 11–25 January, and the period after 25 January. Accordingly, the sudden warming period is partitioned into three stages, namely, precursor stage (1–27 December), rapid warming stage (28 December–10 January), maintaining stage (11–25 January), and decaying stage (after 25 January). In these stages the underlying dynamics are quite different. In the precursor stage, there are two minor short-period warmings (which are more evident at 30 hPa): one between 1 and 7 December and another between 20 and 27 December. This has also been documented in the literature (e.g., Attard et al. 2016; Nath et al. 2016). The SSW-scale APE balances for both warmings are among buoyancy conversion, canonical transfer, and transport. But the energy flow paths are different; hence, two substages may be further distinguished. We choose the following days:

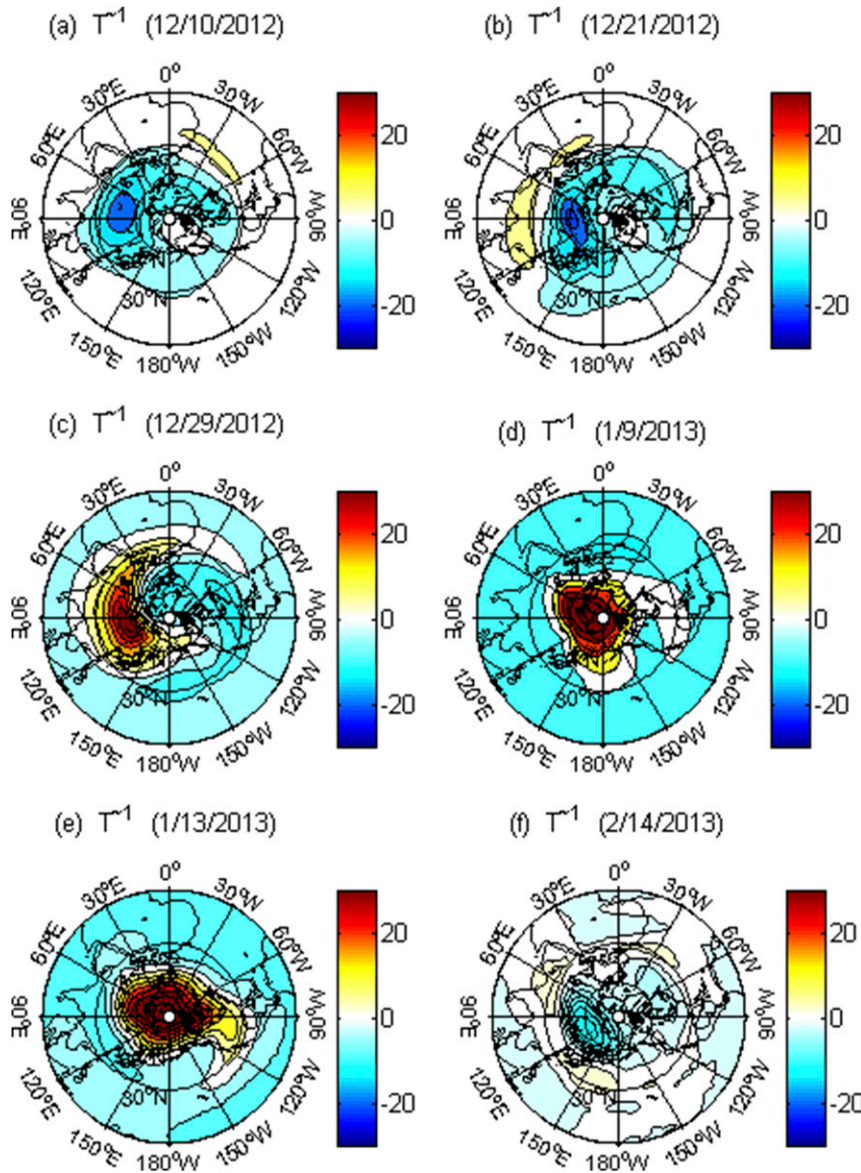


FIG. 6. As in Fig. 4, but for the 10-hPa SSW-scale temperature (K).

3 December (precursor stage, first warming), 22 December (precursor stage, second warming), 4 January (rapid warming stage), 17 January (maintenance stage), and 8 February, which marks the end of the event, to draw the energy flow charts. The results are shown in Fig. 11.

We first examine the precursor stage. The first warming (Fig. 11a) results from the collaboration of the APE transport ΔQ_A^1 and canonical APE transfer from A^0 through a baroclinic instability. The two lead to a flux of 274×10^9 W into A^1 . So, the major energy source for this warming is through the transport ΔQ_A^1 and canonical transfer $\Gamma_A^{0 \rightarrow 1}$, of which a large portion is converted to the kinetic energy on the same scale window.

During the second warming (Fig. 11b), the evolution of the buoyancy conversion is different. Now the growth of A^1 is due to b^1 . It is from K^1 through buoyancy conversion, while K^1 is mainly from K^0 and ΔQ_p^1 . That is to say, ultimately the second minor warming may trace its origin to the sources outside the region through pressure working rate and to the background through canonical transfer.

The rapid warming stage is between late December and early January. Figure 11c depicts the energy flow on a typical day, 4 January. Here the warming is mainly the resultant effect of the canonical transfer from the mean-scale APE reservoir through baroclinic

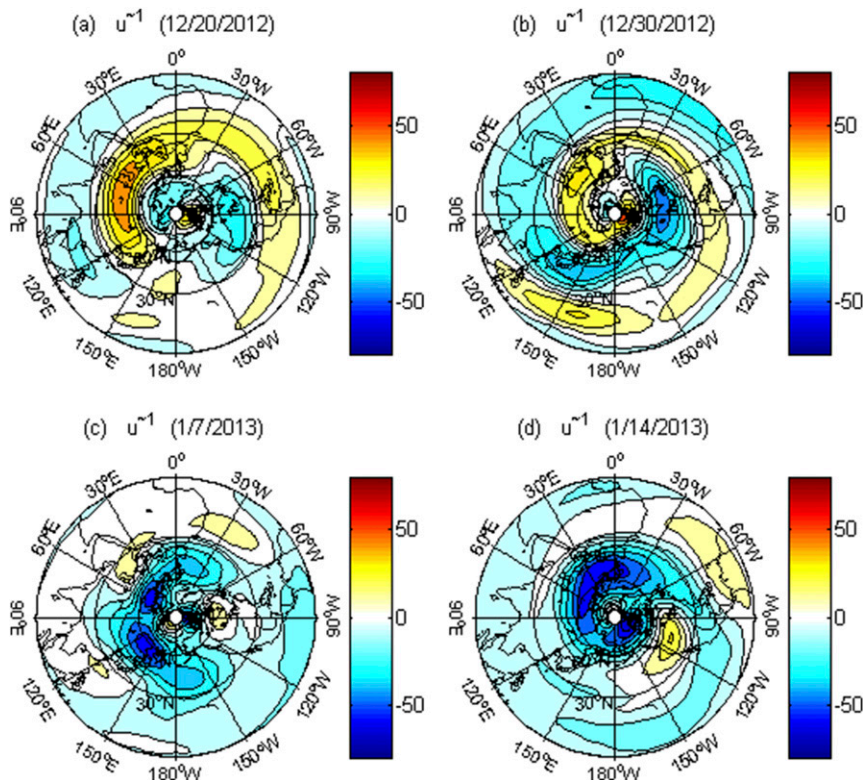


FIG. 7. Time evolution of the 10-hPa SSW-scale zonal wind (m s^{-1}): (a) 20 and (b) 30 Dec 2012, and (c) 7 and (d) 14 Jan 2013.

instability, the SSW-scale APE transport, and the buoyancy conversion on the SSW-scale window. This is similar to the first minor warming, except for their different relative strengths and a reversed canonical transfer between the SSW- and synoptic-scale windows. Here $\Gamma_A^{0 \rightarrow 1}$, $\Gamma_A^{2 \rightarrow 1}$, and ΔQ_A^1 all contribute to the growth of A^1 , and $\Gamma_A^{0 \rightarrow 1} + \Gamma_A^{2 \rightarrow 1} + \Delta Q_A^1 = 832.9 \times 10^9 \text{ W}$. The buoyancy conversion rate b^1 takes $605.0 \times 10^9 \text{ W}$ out of the $832.9 \times 10^9 \text{ W}$. The remaining $227.9 \times 10^9 \text{ W}$ causes the explosive growth of A^1 and hence the rapid rise in temperature. The converted energy has different destinations. It is mainly taken away through advection (ΔQ_K^1) and pressure work (ΔQ_p^1) (the canonical transfer from the mean flow and that to the synoptic eddies are approximately balanced). There is a net influx of $31.0 \times 10^9 \text{ W}$ that, though weak, will make the SSW-scale flow grow. That is to say, in this stage, not all the APE acquired is released to warm the stratosphere; a significant part is stored in the SSW-scale KE for later use.

Followed by the rapid warming stage is the stage of maintenance (Fig. 11d). Compared to the rapid warming stage, the energetic scenario is completely different. Now the balance of the SSW-scale APE is among the following four terms: $\Gamma_A^{0 \rightarrow 1}$, $\Gamma_A^{2 \rightarrow 1}$, ΔQ_A^1 , and b^1 . A major change is that ΔQ_A^1 , and b^1 completely reverse their

directions. Besides, $\Gamma_A^{2 \rightarrow 1}$, the canonical transfer between the SSW and synoptic eddies becomes significant via a secondary baroclinic instability, which almost cancels out the canonical transfer from the mean window through the primary baroclinic instability. So, in this stage the warming is maintained by the energy from SSW-scale KE (i.e., K^1), through buoyancy conversion, though most of the energy thus obtained may be transported away through ΔQ_A^1 .

If we trace further the origin of the SSW-scale KE, we will find that it has two major sources. Recall that the SSW-scale KE has stored a part of the converted SSW-scale APE earlier on, so the first source is actually the SSW-scale APE itself. The second major source is the kinetic energy reservoir on the mean-scale window. From Fig. 11d it is clear that, in this stage, there is a very strong barotropic instability that extracts the energy from K^0 to fuel K^1 , which is then instantaneously converted to A^1 . By the numbers given in the figure, the second source is by far the most important. Since K^0 is mainly supplied through ΔQ_p^0 , the ultimate energy source for the warming in this stage might be due to the upward propagating of the planetary-scale waves, as claimed in the classical paradigm. We will discuss this further below.

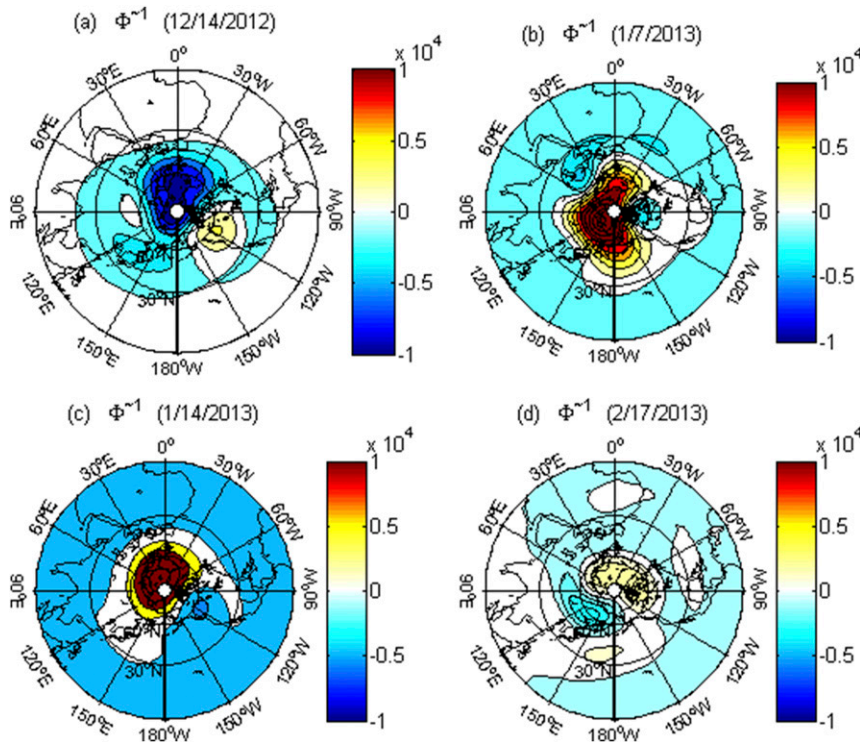


FIG. 8. Time evolution of the 10-hPa SSW-scale geopotential (J kg^{-1}): (a) 14 Dec 2012, (b) 7 and (c) 14 Jan 2013, and (d) 17 Feb 2013.

The final stage is the decaying stage. For example, on 8 February, the energetics are very similar to that in Fig. 11e, but the canonical transfers and buoyancy conversions are all nearly zero.

3) HORIZONTAL DISTRIBUTIONS OF THE INTERSCALE TRANSFER AND BUOYANCY CONVERSION

One of the advantages of the MS-EVA is that it can reveal the spatiotemporal structure of the energetics. Here we integrate the transfers $\Gamma_A^{0 \rightarrow 1}$ and $\Gamma_K^{0 \rightarrow 1}$ and buoyancy

conversion from 100–10 hPa and draw the resulting horizontal distributions in Fig. 12.

In this figure, 4 January is a typical day when $\Gamma_A^{0 \rightarrow 1}$ dominates. In Fig. 12a, most of the polar region has been occupied with positive $\Gamma_A^{0 \rightarrow 1}$, though its distribution is spatially inhomogeneous. That is to say, in the stage of rapid warming, APE is mainly from the mean window to the SSW window through baroclinic instability. The quantity $\Gamma_K^{0 \rightarrow 1}$ is of like importance in the next stage (i.e., the stage of maintenance). On 17 January, there is one strong positive center over Alaska–Canada, while in most other regions,

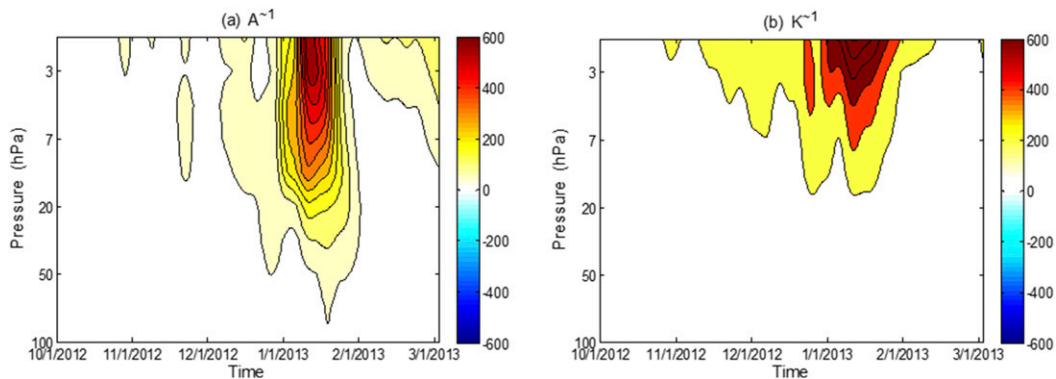


FIG. 9. Time–pressure distributions of the horizontally integrated (over the whole Northern Hemisphere) SSW-scale (a) APE and (b) KE.

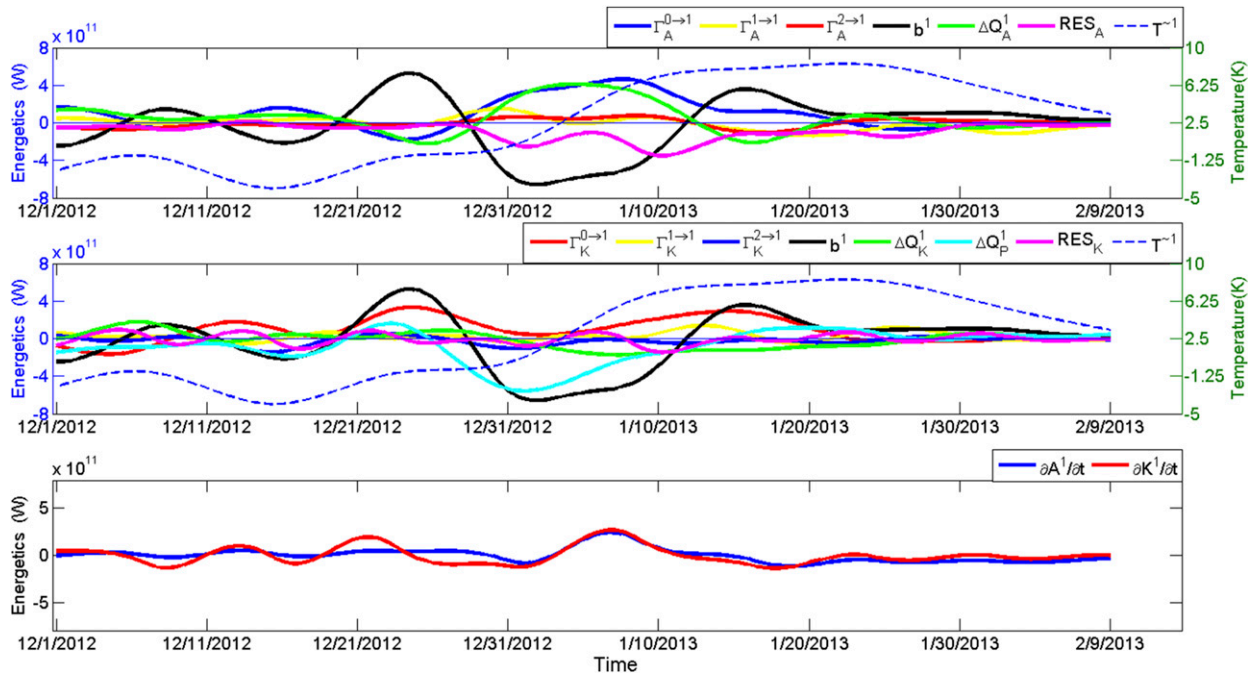


FIG. 10. The balance among the (top) APE and (middle) KE energetics (W) on the SSW-scale window integrated from 60° to 84° N and from 100 to 10 hPa: (top) $\Gamma_A^{0\rightarrow 1}$ (blue), $\Gamma_A^{1\rightarrow 1}$ (red), $\Gamma_A^{2\rightarrow 1}$ (red), b^1 (black), ΔQ_A^1 (green), and T^{-1} (blue dashed); and (middle) $\Gamma_K^{0\rightarrow 1}$ (red), $\Gamma_K^{1\rightarrow 1}$ (yellow), $\Gamma_K^{2\rightarrow 1}$ (blue), b^1 (black), ΔQ_K^1 (green), ΔQ_p^1 (cyan), and T^{-1} (blue dashed). The values RES_A (purple in top) and RES_K (purple in middle) are the residuals for the APE and KE equations, respectively. (bottom) The energy change rates $\partial A^1/\partial t$ (blue) and $\partial K^1/\partial t$ (red).

$\Gamma_K^{0\rightarrow 1}$ takes zero or negative values (Fig. 12b). Figures 12c and 12d are the SSW-scale buoyancy conversion rates b^1 for these two days. Obviously, there is a reversal of direction of b^1 , as described in the preceding subsection, from negative (APE to KE) to positive (KE to APE) values. However, b^1 reverses its direction only over the following regions: Greenland, East Siberia, etc. Over Eurasia and the Canada basin it remains negative.

4) MORE ABOUT THE PRESSURE WORK AND ENERGY TRANSPORTS ON THE SSW WINDOW

With the analysis above, we have seen that b^1 , ΔQ_p^1 , ΔQ_A^1 , $\Gamma_A^{0\rightarrow 1}$, $\Gamma_A^{2\rightarrow 1}$, and indirectly, ΔQ_p^0 , are the major mechanisms involved in the 2013 SSW. Here, ΔQ_p^0 , ΔQ_p^1 , and ΔQ_A^1 are the divergences of three vectors, so we still need to differentiate the roles of the individual components. To do this, we separate a divergence into three parts, each with a component, and repeat the integrations as above. Since the integrals are with respect to the whole zonal band, their zonal components all vanish. For the integral of ΔQ_A^1 , interestingly, the vertical component is also nearly zero. This implies that an important mechanism triggering the sudden warming is the meridional heat transport: particularly, the poleward heat transport. In contrast, the integral of ΔQ_p^1 has both the vertical part and the meridional part, but the former is 3 times bigger. Moreover, the vertical part is upward; that is to say, the

energy supply of K^0 is mainly from the lower atmosphere. For ΔQ_p^1 , before the wind varies, the integral also has both the vertical part and the meridional part. But after the wind varies, the flux that accounts for the growth of K^1 is mainly supplied by the vertical part.

To summarize, the major SSW in December 2012–January 2013 may be divided into three stages. In the rapid warming stage, because of the second precursor stratospheric warming in 20–28 December, part of the energy is stored in A^1 , plus the poleward heat transport and the canonical transfers through the baroclinic instabilities in the polar region, which cause A^1 , and hence the SSW-scale temperature, to grow explosively. A part of the increased A^1 is converted into K^1 , the SSW-scale KE, and hence causes the polar stratospheric circulation to change, resulting in a weak westerly and a strengthened easterly. This makes the rapid warming stage. In the second stage, the system acquires K^1 via barotropic instability. This together with the energy stored in K^1 earlier on is converted back to A^1 through the positive buoyancy conversion over Greenland and East Siberia. The buoyancy conversion collaborates with the canonical baroclinic transfer from the mean-scale window (through baroclinic instability) to increase A^1 , maintaining the warming to an appreciable extent. [We remark that this stage dependence of dynamical processes has also been observed in other

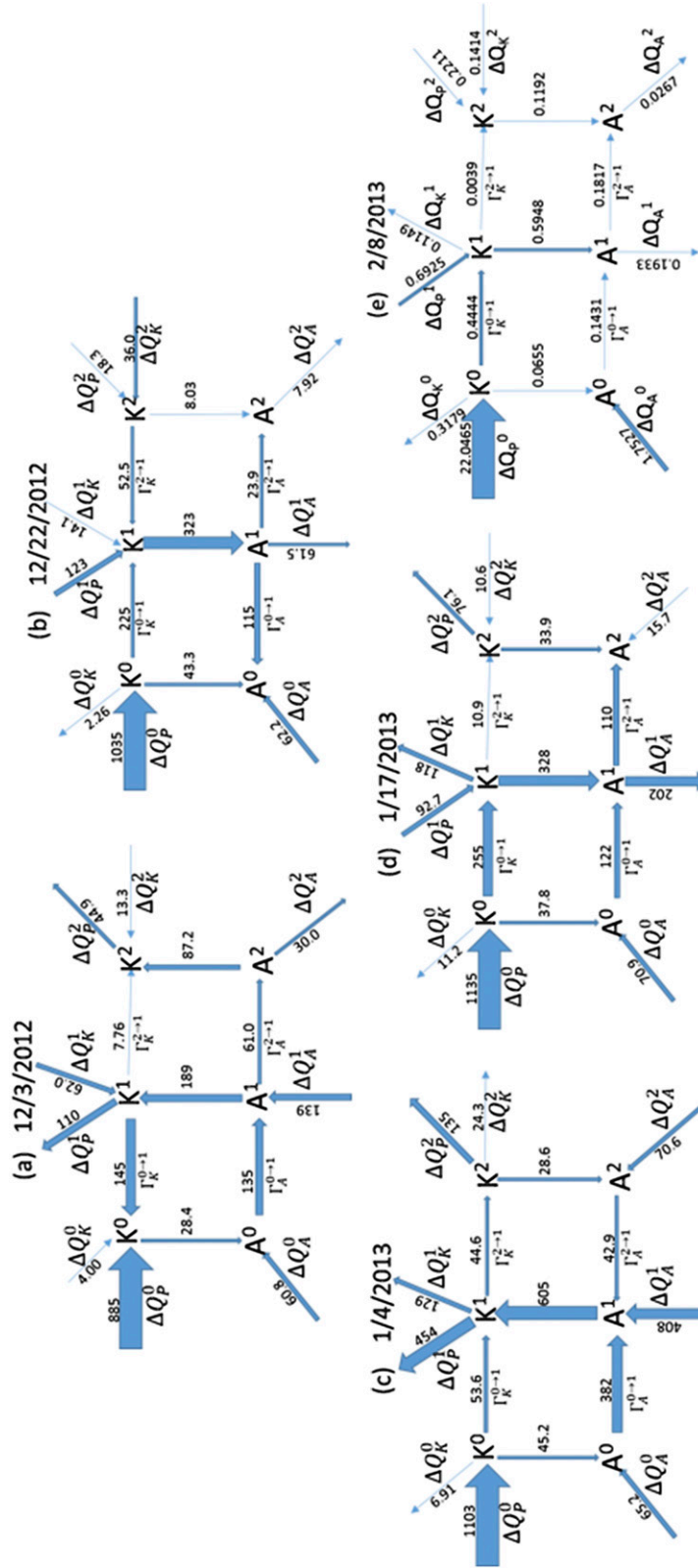


FIG. 11. The typical multiscale energy cycles (10^9 W) for (a), (b) the precursor stage (3 and 22 Dec, respectively); (c) rapid warming stage (4 Jan); (d) maintaining stage (17 Jan); and (e) decaying stage (8 Feb).

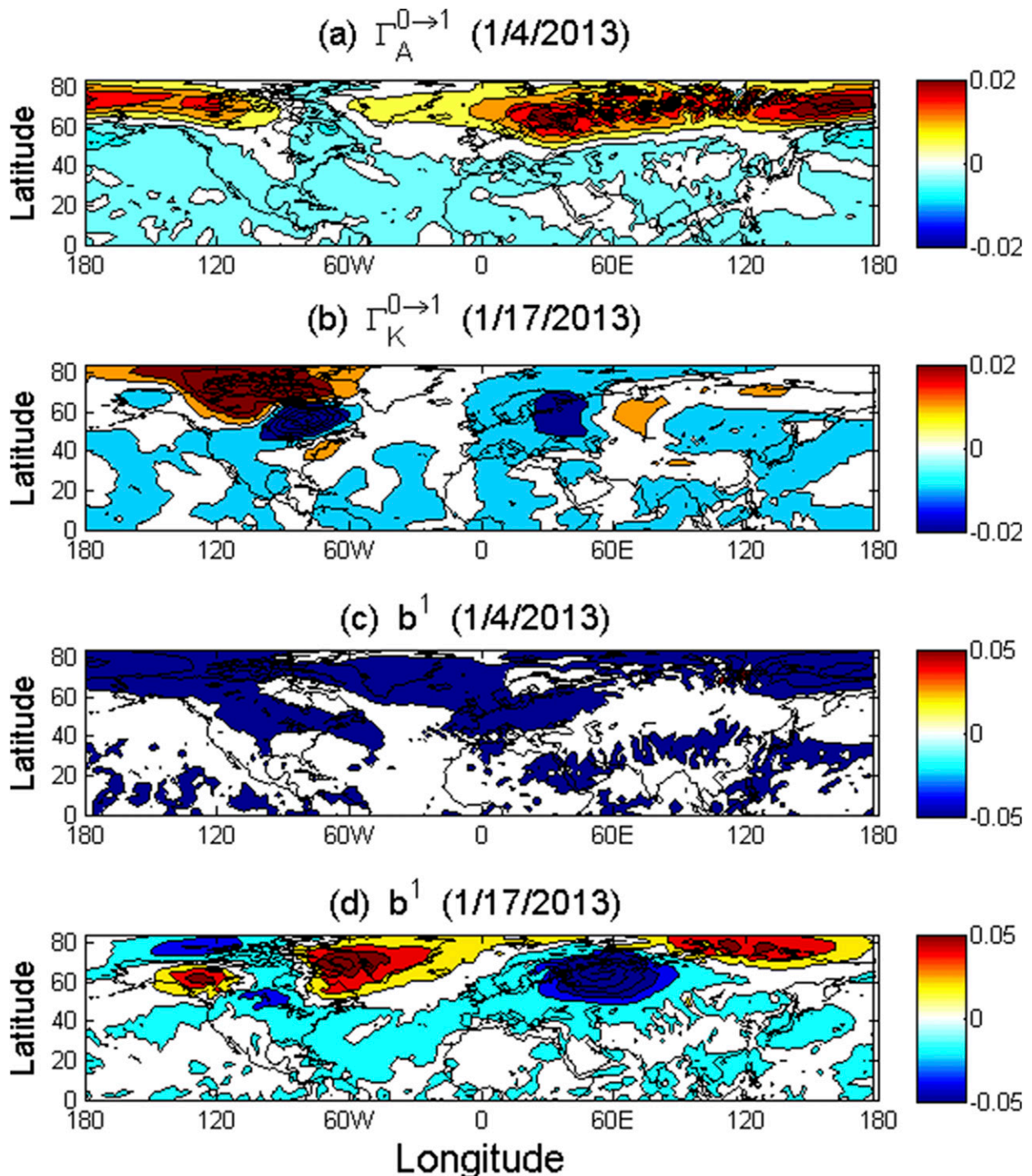


FIG. 12. (a) The canonical transfer of APE (10^9 W) from the mean window to the SSW-scale window on a typical day of the rapid warming stage (4 Jan). (b) As in (a), but for KE on a day of the maintenance stage (17 Jan). (c),(d) The buoyancy conversions on the above two days, respectively.

phenomena, such as atmospheric blockings (Ma and Liang 2017).] It is important to note that positive buoyancy conversion does not always exist throughout the polar region, while the warming is much more

uniformly distributed, though originally it appears only over the Eurasian continent. So how is energy transported from one place to another place? To see this, we draw in Fig. 13 the horizontal vectors of the SSW-scale

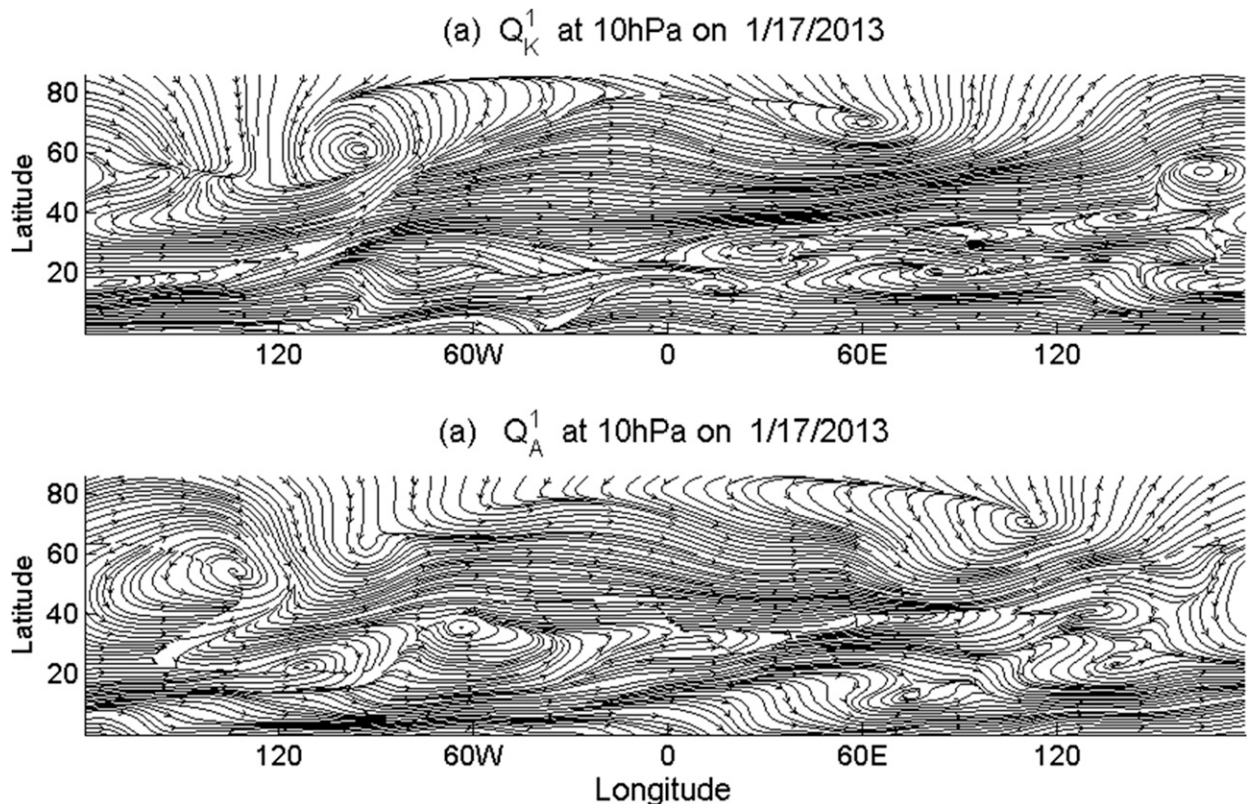


FIG. 13. The horizontal SSW-scale (top) KE and (bottom) APE flux on 17 Jan 2013.

KE and APE transports. Clearly, after the warming starts, both Q_A^1 and Q_K^1 display cyclonic–anticyclonic patterns on the two continents. Recall that the buoyancy conversion mostly occurs in these regions. Further notice that, over the Bering Strait and Norwegian Sea, the vectors are generally eastward. They connect the two continents, making the SSW-scale energy acquired from different mechanisms throughout the polar region. As time moves on, the two SSW-scale cyclonic circulations become weaker and weaker until they disappear.

7. Conclusions

The December 2012–January 2013 sudden stratospheric warming (SSW) lasts for an extraordinarily long time. It is special in that, prior to the major warming, there exist two minor warmings in December 2012; moreover, the polar vortex is not only displaced, but also split. This study uses a recently developed tool, multiscale window transform (MWT), and the MWT-based localized multiscale energy and vorticity analysis (MS-EVA). The fields are reconstructed on three orthogonal subspaces or scale windows [i.e., mean window, sudden warming window (or SSW window), and

synoptic-scale window]. The warming event is much clearer in the SSW-scale reconstructions than in the original fields. Particularly, on the SSW-scale window, the temperature evolution appears as an almost solitary warming center around the North Pole, in contrast to the dipolar or multipolar pattern in the original temperature maps.

We denote the multiscale available potential energy (APE) and kinetic energy (KE) as, respectively, A^ϖ and K^ϖ , where the superscripts $\varpi = 0, 1, 2$ signify the mean window, SSW window, and synoptic-scale window. It is found that the whole period of the major warming may be divided into three stages: namely, the rapid warming stage, the maintaining stage, and the decaying stage, each with different controlling dynamics. In the rapid warming stage (28 December–10 January), the system has already gained some A^1 , thanks to the minor warming prior to it. Because of the strong poleward flux of heat and the canonical transfer through baroclinic instabilities that extract APE from A^0 , A^1 , and hence the SSW-scale temperature, grows explosively. In what follows, a large part of the acquired energy is converted to K^1 via buoyancy conversion, leading to an abrupt change in the polar stratospheric circulation, which reverses the polar night jet. Considering the buoyancy

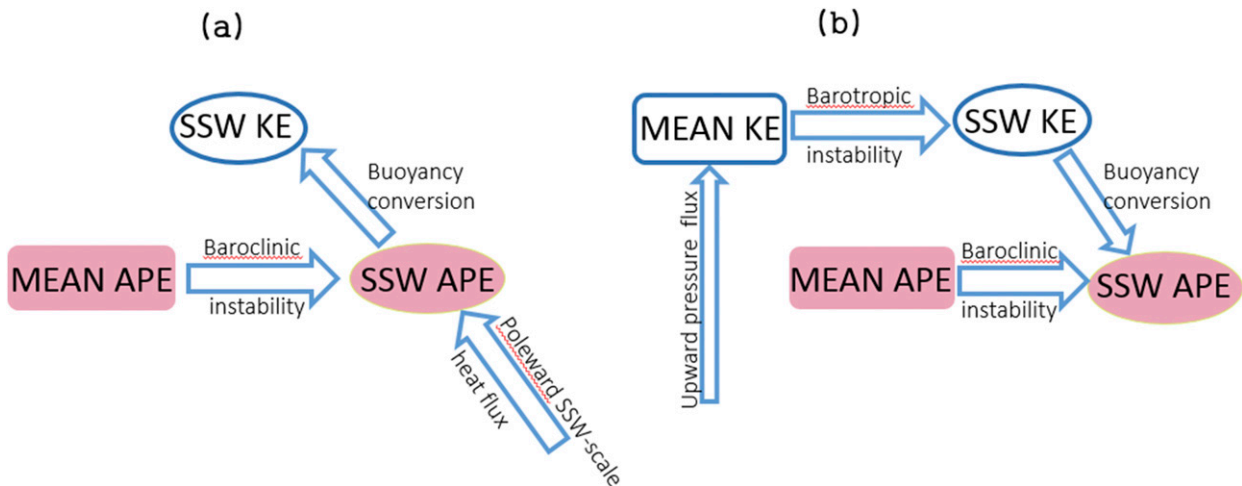


FIG. 14. Schematic of the major processes that lead to the January 2013 sudden stratospheric warming. (a) In the stage of rapid warming (28 Dec–10 Jan), the temperature rise is mainly due to a strong poleward heat flux and a canonical transfer through baroclinic instability, which extracts APE from the mean window. In the meantime, a portion of the SSW-scale APE is converted to the SSW-scale KE. (b) In the stage of maintenance (11–25 Jan), the previously converted energy is converted back; a strong barotropic instability transfers the mean-scale KE to the SSW-scale KE, which is also converted to the SSW-scale APE. The mean-scale KE is mostly brought upward from the troposphere by pressure work.

conversion direction (from A^1 to K^1), in this stage the upward propagation of the planetary waves is not the cause of the warming. Instead, the warming comes from the background APE through baroclinic instability and the strong poleward flux of heat.

The strong poleward heat flux is also seen in other energetics studies, such as Julian and Labitzke (1965). Note that sometimes a meridional eddy heat flux may result from an upward-propagating planetary wave. But in this case this flux cannot be due to mechanisms that originated in the troposphere. We examined the vertical integrals of the energetics from 100 to 10 hPa and found that the vertical component of the pressure work is small and, moreover, is downward. That is to say, the heat flux can only be due to processes within the stratosphere, among which meridional advection must play a role.

In the next stage (11–25 January; i.e., the stage of maintenance) the mechanism for the warming is completely different; the SSW-scale APE is from the SSW-scale KE, or K^1 . Here, K^1 includes three parts: 1) the previously converted energy stored in K^1 , 2) the energy newly acquired through pressure work, and, 3) most importantly, that released from the mean-scale window through a strong barotropic instability over Alaska. Since the mean-scale KE reservoir is mainly from the pressure work on this window and the pressure work has a large vertical component, the energy for the warming in this stage should be from the lower atmosphere.

In the decay stage, the energy flow takes a path similar to the maintenance stage, but now the canonical transfers and buoyancy conversions are all nearly

turned off. Accordingly, the system gradually resumes its normal state.

To summarize, the above processes are schematized in Fig. 14. Of particular interest are the reversal of the buoyancy conversion and the appearance of the barotropic instability in the stage of the maintenance. Besides, the poleward SSW-scale heat flux and the upward pressure flux also distinguish the two stages. We remark that the dynamical scenario in the rapid warming stage is consistent with an intrinsic mechanism (e.g., the self-tuned resonance theory) but excludes the mechanism of upward planetary wave driving because the buoyancy conversion on the SSW-scale window is from APE to KE. This is in contrast to the stage of maintenance, when the scenario admits the classical theory of mean flow–wave interaction with the upward-propagating waves. This study provides for the first time, an example that the two completely different types of generating mechanisms proposed so far—i.e., the interaction with the upward-propagating waves (Charney and Drazin 1961; Matsuno 1970) and the intrinsic mechanisms, such as self-tuned resonance (Plumb 1981; McIntyre 1982; Dritschel and McIntyre 2008; Esler and Matthewman 2011; Matthewman and Esler 2011; Albers and Birner 2014)—might actually work together to drive the same event. Some mechanisms, such as the strong barotropic instability over Alaska–Canada and the backward conversion of the previously converted SSW-scale APE, among others, are also first seen. These results, though obtained with an individual case, may help to trace the origins of the

SSWs and build up our knowledge of this important dynamical phenomenon.

Several issues remain. First, one naturally may wonder how the above analysis could help to improve SSW prediction. A possible approach is, based on the energetic flow, to identify the important precursor regions; as an example, Garfinkel and Waugh (2014) suggested the importance of the North Pacific. Second, the 2012/13 SSW might not be representative in that it involves both vortex splits and vortex displacements, and that could be the reason why both mechanisms coexist in this single event. To gain a general understanding of the multiscale energetics underlying a typical SSW, an MS-EVA analysis of all the SSWs, followed by a composite analysis, is needed. These problems, among others, will be explored in future studies.

Acknowledgments. The comments and suggestions from three anonymous referees are sincerely appreciated. We thank ECMWF for making available the ERA-Interim product. This work was partially supported by the 2015 Jiangsu Program of Entrepreneurship and Innovation Group, by the National Science Foundation of China (NSFC) under Grant 41276032, by the National Program on Global Change and Air–Sea Interaction (GASI-IPOVAI-06), and by the Jiangsu Chair Professorship to X.S.L.

REFERENCES

- Albers, J. R., and T. Birner, 2014: Vortex preconditioning due to planetary and gravity waves prior to sudden stratospheric warmings. *J. Atmos. Sci.*, **71**, 4028–4054, doi:10.1175/JAS-D-14-0026.1.
- Attard, H. E., R. Riosberrios, C. T. Guastini, and A. L. Lang, 2016: Tropospheric and stratospheric precursors to the January 2013 sudden stratospheric warming. *Mon. Wea. Rev.*, **144**, 1321–1339, doi:10.1175/MWR-D-15-0175.1.
- Baldwin, M. P., and T. J. Dunkerton, 2001: Stratospheric harbingers of anomalous weather regimes. *Science*, **294**, 581–584, doi:10.1126/science.1063315.
- Batchelor, G. k., 1953: *The Theory of Homogeneous Turbulence*. Cambridge University Press, 197 pp.
- Black, R. X., and B. A. McDaniel, 2007: The dynamics of Northern Hemisphere stratospheric final warming events. *J. Atmos. Sci.*, **64**, 2932–2946, doi:10.1175/JAS3981.1.
- , —, and W. A. Robinson, 2006: Stratosphere–troposphere coupling during spring onset. *J. Climate*, **19**, 4891–4901, doi:10.1175/JCLI3907.1.
- Butler, A. H., L. M. Polvani, and C. Deser, 2014: Separating the stratospheric and tropospheric pathways of El Niño–Southern Oscillation teleconnections. *Environ. Res. Lett.*, **9**, 024014, doi:10.1088/1748-9326/9/2/024014.
- , D. J. Seidel, S. C. Hardiman, N. Butchart, T. Birner, and A. Match, 2015: Defining sudden stratospheric warmings. *Bull. Amer. Meteor. Soc.*, **96**, 1913–1928, doi:10.1175/BAMS-D-13-00173.1.
- Chao, W. C., 1985: Sudden stratospheric warmings as catastrophes. *J. Atmos. Sci.*, **42**, 1631–1646, doi:10.1175/1520-0469(1985)042<1631:SSWAC>2.0.CO;2.
- Charney, J. G., and P. G. Drazin, 1961: Propagation of planetary-scale disturbances from the lower into the upper atmosphere. *J. Geophys. Res.*, **66**, 83–109, doi:10.1029/JZ066i001p00083.
- Charyulu, D. V., V. Sivakumar, H. Bencherif, and G. Kirgis, 2007: 20-year lidar observations of stratospheric sudden warming over a mid-latitude site, Observatoire de Haute Provence (Ohp; 44°N, 6°E): Case study and statistical characteristics. *Atmos. Chem. Phys.*, **7**, 15 739–15 779, doi:10.5194/acpd-7-15739-2007.
- Coy, L., K. Warga, G. L. Manney, and S. Pawson, 2015: The major stratospheric sudden warming of January 2013: Analyses and forecasts in the GEOS-5 data assimilation system. *Mon. Wea. Rev.*, **143**, 491–510, doi:10.1175/MWR-D-14-00023.1.
- De Wit, R. J., R. E. Hibbins, P. J. Espy, and E. A. Hennem, 2015: Coupling in the middle atmosphere related to the 2013 major sudden stratospheric warming. *Ann. Geophys.*, **33**, 309–319, doi:10.5194/angeo-33-309-2015.
- Dickinson, R. E., 1968: Planetary Rossby waves propagating vertically through weak westerly wind wave guides. *J. Atmos. Sci.*, **25**, 984–1002, doi:10.1175/1520-0469(1968)025<0984:PRWPVT>2.0.CO;2.
- Dritschel, D. G., and M. E. McIntyre, 2008: Multiple jets as PV staircases: The Phillips effect and the resilience of eddy-transport barriers. *J. Atmos. Sci.*, **65**, 855–874, doi:10.1175/2007JAS2227.1.
- Esler, J. G., and N. J. Matthewman, 2011: Stratospheric sudden warmings as self-tuning resonances. Part II: Vortex displacement events. *J. Atmos. Sci.*, **68**, 2505–2523, doi:10.1175/JAS-D-11-08.1.
- Garfinkel, C. I., and D. W. Waugh, 2014: Tropospheric Rossby wave breaking and variability of the latitude of the eddy-driven jet. *J. Climate*, **27**, 7069–7085, doi:10.1175/JCLI-D-14-00081.1.
- Gray, L. J., S. Crooks, C. Pascoe, S. Sparrow, and M. Palmer, 2004: Solar and QBO influences on the timing of stratospheric sudden warmings. *J. Atmos. Sci.*, **61**, 2777–2796, doi:10.1175/JAS-3297.1.
- Harada, Y., A. Goto, H. Hasegawa, N. Fujikawa, H. Naoe, and T. Hirooka, 2010: A major stratospheric sudden warming event in January 2009. *J. Atmos. Sci.*, **67**, 2052–2069, doi:10.1175/2009JAS3320.1.
- Hitchcock, P., and I. R. Simpson, 2016: Quantifying eddy feedbacks and forcings in the tropospheric response to stratospheric sudden warmings. *J. Atmos. Sci.*, **73**, 3641–3657, doi:10.1175/JAS-D-16-0056.1.
- Holopainen, E. O., 1978: A diagnostic study on the kinetic energy balance of the long-term mean flow and the associated transient fluctuations in the atmosphere. *Geophysica*, **15**, 125–145.
- Holton, J. R., 1976: A semi-spectral numerical model for wave-mean flow interactions in the stratosphere—Application to sudden stratospheric warmings. *J. Atmos. Sci.*, **33**, 1639–1649, doi:10.1175/1520-0469(1976)033<1639:ASSNMF>2.0.CO;2.
- , 1980: The dynamics of sudden stratospheric warmings. *Annu. Rev. Earth Planet. Sci.*, **8**, 169–190, doi:10.1146/annurev.ea.08.050180.001125.
- Ineson, S., and A. A. Scaife, 2009: The role of the stratosphere in the European climate response to El Niño. *Nat. Geosci.*, **2**, 32–36, doi:10.1038/ngeo381.
- Jiang, X., J. Wang, E. T. Olsen, T. Pagano, L. L. Chen, and Y. L. Yung, 2013: Influence of stratospheric sudden warming

- on AIRS midtropospheric CO₂. *J. Atmos. Sci.*, **70**, 2566–2573, doi:10.1175/JAS-D-13-064.1.
- Julian, P. R., and K. B. Labitzke, 1965: A study of atmospheric energetics during the January–February 1963 stratospheric warming. *J. Atmos. Sci.*, **22**, 597–610, doi:10.1175/1520-0469(1965)022<0597:ASOAE>2.0.CO;2.
- Kodera, K., 2006: Influence of stratospheric sudden warming on the equatorial troposphere. *Geophys. Res. Lett.*, **33**, L06804, doi:10.1029/2005GL024510.
- Liang, X. S., 2016: Canonical transfer and multiscale energetics for primitive and quasi-geostrophic atmospheres. *J. Atmos. Sci.*, **73**, 4439–4468, doi:10.1175/JAS-D-16-0131.1.
- , and M. Wang, 2004: A study of turbulent wakes using a novel localized stability analysis. *Proc. Center for Turbulence Research Summer Program 2004*, Stanford, CA, Stanford–NASA Ames Research Center, 211–222.
- , and A. R. Robinson, 2005: Localized multiscale energy and vorticity analysis: I. Fundamentals. *Dyn. Atmos. Oceans*, **38**, 195–230, doi:10.1016/j.dynatmoce.2004.12.004.
- , and D. G. M. Anderson, 2007: Multiscale window transform. *SIAM J. Multiscale Model. Simul.*, **6**, 437–467, doi:10.1137/06066895X.
- , and A. R. Robinson, 2007: Localized multiscale energy and vorticity analysis: II. Finite-amplitude instability theory and validation. *Dyn. Atmos. Oceans*, **44**, 51–76, doi:10.1016/j.dynatmoce.2007.04.001.
- Liu, Y., and Y. Zhang, 2014: Overview of the major 2012–13 Northern Hemisphere stratospheric sudden warming: Evolution and its association with surface weather. *J. Meteor. Res.*, **28**, 561–575, doi:10.1007/s13351-014-3065-z.
- Lorenz, E. N., 1955: Available potential energy and the maintenance of the general circulation. *Tellus*, **7**, 157–167, doi:10.3402/tellusa.v7i2.8796.
- Ma, J., and X. S. Liang, 2017: Multiscale dynamical processes underlying the wintertime Atlantic blockings. *J. Atmos. Sci.*, doi:10.1175/JAS-D-16-0295.1, in press.
- Matsuno, T., 1970: Vertical propagation of stationary planetary waves in the winter Northern Hemisphere. *J. Atmos. Sci.*, **27**, 871–883, doi:10.1175/1520-0469(1970)027<0871:VPOSPW>2.0.CO;2.
- , 1971: A dynamical model of the stratospheric sudden warming. *J. Atmos. Sci.*, **28**, 1479–1494, doi:10.1175/1520-0469(1971)028<1479:ADMOTS>2.0.CO;2.
- Matthewman, N. J., and J. G. Esler, 2011: Stratospheric sudden warmings as self-tuning resonances. Part I: Vortex splitting events. *J. Atmos. Sci.*, **68**, 2481–2504, doi:10.1175/JAS-D-11-07.1.
- McInturff, R. M., Ed., 1978: Stratospheric warmings: Synoptic, dynamic and general-circulation aspects. NASA Reference Publ. NASA-RP-1017, 174 pp. [Available online at <http://ntrs.nasa.gov/archive/nasa/casi.ntrs.nasa.gov/19780010687.pdf>].
- McIntyre, M. E., 1982: How well do we understand the dynamics of stratospheric warmings? *J. Meteor. Soc. Japan*, **60**, 37–65, doi:10.2151/jmsj1965.60.1_37.
- Murakami, S., 2011: Atmospheric local energetics and energy interactions between mean and eddy fields. Part I: Theory. *J. Atmos. Sci.*, **68**, 760–768, doi:10.1175/2010JAS3664.1.
- Nath, D., W. Chen, C. Zelin, A. I. Pogoreltsev, and K. Wei, 2016: Dynamics of 2013 sudden stratospheric warming event and its impact on cold weather over Eurasia: Role of planetary wave reflection. *Sci. Rep.*, **6**, 24174, doi:10.1038/srep24174.
- O’Neill, A., A. J. Charlton-Perez, and L. M. Polvani, 2015: Middle atmosphere: Stratospheric sudden warmings. *Encyclopedia of Atmospheric Sciences*. Vol. 3, Elsevier, 30–40, doi:10.1016/B978-0-12-382225-3.00230-9.
- Perry, J. S., 1967: Long-wave energy processes in the 1963 sudden stratospheric warming. *J. Atmos. Sci.*, **24**, 539–550, doi:10.1175/1520-0469(1967)024<0539:LWEPIT>2.0.CO;2.
- Plumb, R. A., 1981: Instability of the distorted polar night vortex: A theory of stratospheric warmings. *J. Atmos. Sci.*, **38**, 2514–2531, doi:10.1175/1520-0469(1981)038<2514:IOTDPN>2.0.CO;2.
- , 1983: A new look at the energy cycle. *J. Atmos. Sci.*, **40**, 1669–1688, doi:10.1175/1520-0469(1983)040<1669:ANLATE>2.0.CO;2.
- Pope, S. B., 2003: *Turbulent Flows*. Cambridge University Press, 771 pp.
- Reed, R. J., J. L. Wolfe, and H. Nishimoto, 1963: A spectral analysis of the energetics of the stratospheric sudden warming of early 1957. *J. Atmos. Sci.*, **20**, 256–275, doi:10.1175/1520-0469(1963)020<0256:ASAOTE>2.0.CO;2.
- Reichler, T., J. Kim, E. Manzini, and J. Kröger, 2012: A stratospheric connection to Atlantic climate variability. *Nat. Geosci.*, **5**, 783–787, doi:10.1038/ngeo1586.
- Robinson, W. A., 1985: A model of the wave 1–wave 2 vacillation in the winter stratosphere. *J. Atmos. Sci.*, **42**, 2289–2304, doi:10.1175/1520-0469(1985)042<2289:AMOTWV>2.0.CO;2.
- , 1988: Irreversible wave–mean flow interactions in a mechanistic model of the stratosphere. *J. Atmos. Sci.*, **22**, 3413–3430, doi:10.1175/1520-0469(1988)045<3413:IWFHIA>2.0.CO;2.
- Schoeberl, M. R., and D. L. Hartmann, 1991: The dynamics of the stratospheric polar vortex and its relation to springtime ozone depletions. *Science*, **251**, 46–52, doi:10.1126/science.251.4989.46.
- Sheshadri, A., R. A. Plumb, and D. I. V. Domeisen, 2014: Can the delay in Antarctic polar vortex breakup explain recent trends in surface westerlies? *J. Atmos. Sci.*, **71**, 566–573, doi:10.1175/JAS-D-12-0343.1.
- Sjoberg, J. P., and T. Birner, 2012: Transient tropospheric forcing of sudden stratospheric warmings. *J. Atmos. Sci.*, **69**, 3420–3432, doi:10.1175/JAS-D-11-0195.1.
- Strang, G., and T. Nguyen, 1997: *Wavelets and Filter Banks*. Wellesley-Cambridge Press, 520 pp.
- Taguchi, M., 2016: Predictability of major stratospheric sudden warmings: Analysis results from JMA operational 1-month ensemble predictions from 2001/02 to 2012/13. *J. Atmos. Sci.*, **73**, 789–806, doi:10.1175/JAS-D-15-0201.1.
- Thompson, D. W. J., M. P. Baldwin, and J. M. Wallace, 2002: Stratospheric connection to Northern Hemisphere wintertime weather: Implications for prediction. *J. Climate*, **15**, 1421–1428, doi:10.1175/1520-0442(2002)015<1421:SCTNHW>2.0.CO;2.
- Trenberth, K. E., 1973: Dynamic coupling of the stratosphere with the troposphere and sudden stratospheric warmings. *Mon. Wea. Rev.*, **101**, 306–322, doi:10.1175/1520-0493(1973)101<0306:DCOTSW>2.3.CO;2.
- Tripathi, O. P., and Coauthors, 2016: Examining the predictability of the stratospheric sudden warming of January 2013 using multiple NWP systems. *Mon. Wea. Rev.*, **144**, 1935–1960, doi:10.1175/MWR-D-15-0010.1.
- Zuo, Q., S. Gao, and D. Lü, 2012: Kinetic and available potential energy transport during the stratospheric sudden warming in January 2009. *Adv. Atmos. Sci.*, **29**, 1343–1359, doi:10.1007/s00376-012-1198-5.